Analyst

Cite this: *Analyst*, 2011, **136**, 2111

www.rsc.org/analyst

PAPER

Probing the binding kinetics of proinflammatory cytokine–antibody interactions using dual color fluorescence cross correlation spectroscopy

Chia-Yan Wu,[a] Chuan-Keng Huang,†[b] Chao-Yu Chung,†[d] I-Ping Huang,[c] Yeukuang Hwu,[e] Chung-Shi Yang,[f] Yiu-Kay Lai,[c] Leu-Wei Lo*[a] and Su-Yu Chiang*[d]

Received 13th December 2010, Accepted 8th March 2011
DOI: 10.1039/c0an00995d

Dual color fluorescence cross correlation spectroscopy (FCCS) was used to investigate quantitatively the binding kinetics of tumor necrosis factor (TNFα) with TNFα antibody (anti-TNFα) following fluorescent labeling. Through the analysis of the auto correlation curves of fluorescence correlation spectroscopy (FCS), diffusion coefficients of 100.06 ± 4.9 $\mu m^2 s^{-1}$ and 48.96 ± 2.52 $\mu m^2 s^{-1}$ for Alexa488-TNFα and Atto647N-anti-TNFα were obtained. In addition, the calculated hydrodynamic diameters of the Alexa488-TNFα and Atto647N-anti-TNFα were approximately 4.89 ± 0.24 nm and 9.99 ± 0.52 nm, respectively, which agrees with the values of 5.20 ± 1.23 nm and 9.28 ± 0.86 nm for the native TNFα and the anti-TNFα as determined from dynamic light scattering measurements. For the binding kinetics, association (k_{on}) and dissociation (k_{off}) rate constants were (1.13 ± 0.08) × 10^4 $M^{-1} s^{-1}$ and (1.53 ± 0.19) × 10^{-3} s^{-1} while the corresponding dissociation constant (K_d) at 25 °C was (1.36 ± 0.10) × 10^{-7} M. We believe this is the first report on the binding kinetics for TNFα-antibody recognition in the homogeneous phase. Using this technology, we have shown that controlled experiments can be performed to gain insight into molecular mechanisms involved in the immune response.

1. Introduction

Cytokines play important roles in regulating the host's responses to infection. They are involved in immune responses, inflammation, and trauma. Some proinflammatory cytokines weaken the disease whereas other anti-inflammatory cytokines serve to reduce inflammation and facilitate healing. Tumor necrosis factor (TNFα) is one of the important immunity-modulating cytokines secreted by several cell types (macrophages, T cells, B cells, endothelial cells, fibroblasts, and cardiomyocytes). It is required by the human body for defense against infectious diseases and carcinogenesis. Low concentrations of TNFα may be important in the host system's response to stress, but excess production appears to be deleterious to the host and causes various autoimmune diseases. TNFα receptors (TNFR1 and TNFR2) with multiple high affinities on specific cell surfaces[1,2] can mediate the biological activities of TNFα by activating diverse signaling pathways or regulating cell survival, proliferation, differentiation, or death. Structurally, TNFα forms multimeric complexes and the biologically active native form is reportedly a trimeric form in solution. However, soluble bioactive 51 kDa trimeric TNFα protein tends to slowly dissociate into monomeric subunits at concentrations below the nanomolar range, thereby losing its bioactivity.[3]

Certainly, detection of abnormal concentrations of TNFα often indicates the presence of various cancers or disease. Numerous reports have demonstrated the role of TNFα as a proinflammatory cytokine, and pointed out the increasing TNFα expression levels in pre-cancerous and tumor cells which were frequently associated with the progression of malignant diseases. Blocking TNFα has been highly successful in patients with autoinflammatory diseases,[4–6] such as rheumatoid arthritis, ankylosing spondylitis, Crohn's disease, septic shock, inflammatory bowel disease, or graft-host disease. In order to treat these inflammatory diseases, previous researchers have reported the use of TNFα antibodies (anti-TNFα) and soluble TNFα receptors (TNFR), which interfere with the activities of TNFα molecules.

Owing to the extreme low cytokine concentrations in the physiological environment, an ultrasensitive detection system

[a]*Division of Medical Engineering Research, National Health Research Institutes, Zhunan, Miaoli 35053, Taiwan ROC. E-mail: lwlo@nhri.org.tw; Fax: +886-37-586440; Tel: +886-37-246166 x37115*
[b]*Department of Applied Chemistry, National Chiao Tung University, Hsinchu 30010, Taiwan ROC*
[c]*Institute of Biotechnology, National Tsing Hua University, Hsinchu 30076, Taiwan ROC*
[d]*National Synchrotron Radiation Research Center, 101, Hsin Ann Road, Science-Based Industrial Park, Hsinchu 30076, Taiwan ROC. E-mail: schiang@nsrrc.org.tw; Fax: +886-3-5789816; Tel: +886-3-5780281 x7315*
[e]*Institute of Physics, Academia Sinica, Taipei 11529, Taiwan ROC*
[f]*Center for Nanomedicine Research, National Health Research Institutes, Zhunan, Miaoli 35053, Taiwan ROC*
† Contributed equally to this work.

possessing single-molecule detection under homogeneous conditions is required. Among fluorescence-based techniques, fluorescence correlation spectroscopy (FCS) is a suitable optical method for investigating the binding kinetics of TNFα and its antibody in minute concentrations. FCS is based on temporal correlation of the intensity fluctuation of fluorescent molecules diffusing in and out of an illuminated focal volume. By analyzing the correlation curves of FCS, one can determine the number of molecules and diffusion times in the confined volume.[7,8] The FCS technique has been extensively applied to the study of measurements of molecular diffusion coefficients,[9–13] molecular pH-dependent relaxation dynamics of enhanced green fluorescent proteins (EGFPs),[14] protein folding dynamics,[15] and conformational changes of nucleic acids.[16] Not only can FCS be used in the chemical kinetics and dynamics of the solution phase, but it can also be used to investigate the diffusion behavior in cell membranes,[17] in the cytosol,[18] and the nucleus.[19] However, FCS can only differentiate diffusion coefficients that have at least a factor difference of 1.6,[20] which corresponds to a 4-fold difference in molecular weights. To overcome this limitation, Eigen and Rigler[21] first proposed the concept of fluorescence cross correlation spectroscopy (FCCS) which is performed by correlating the intensity fluctuations of two different molecular species. Its ensuing biomedical application was reported by Schwille *et al.*,[22] who demonstrated the DNA–DNA hybridization kinetics by using FCCS.

Real time monitoring of biospecific interactions is important for studying the interaction among biomolecules and understanding the relationships between their structures and functions.[23–25] Biotin and streptavidin molecules are typically chosen as an ideal system to demonstrate ligand–receptor interactions due to their high binding association constant ($K_{eq} \approx 10^{15}$ M^{-1})[26] and a slow dissociation rate constant for biotin ($k_{off} \approx 5 \times 10^{-6}$ s^{-1}). Recently, FCS had been applied to investigate the protein–receptor interactions in biophysical and biochemical processes *in vitro*. Varghese *et al.*[27] studied the binding of IgG and Fab fragment of anti-IgG molecules and estimated the dissociation binding constant (K_d) of 15 ± 2 nM using dual color fluorescence FCCS. Fujii *et al.*[28] developed a method for the detection of prion protein and measured the dissociation binding constant (K_d), which was close to 10^{-9} M (at 25 °C), using FCS and FCCS. These studies show that the equilibrium constants of these binding reactions are close to the order of 10^9–10^{11} M^{-1}, which represent a high binding affinity, to form the most stable complexes. Nevertheless, the detection limit of FCCS is also highly related to the small k_{off} of the binding pair.

Although different quantitative results of TNFα in biological fluids can be obtained using bioassay and immunoassay, few studies have reported the kinetic analysis of TNFα. More recently, the technique of surface plasmon resonance (SPR) has been utilized to investigate the binding kinetics of TNFα and its antibody at the solid–liquid phase. Battaglia *et al.*[29] studied the binding kinetics in TNFα and anti-TNFα, and reported an equilibrium dissociation constant of 1.22×10^{-9} M. On the other hand, using a quartz crystal microbalance biosensor integrated in a flow injection analysis system, Liu *et al.*[30] identified the equilibrium dissociation constant as $2.3 \sim 5.4 \times 10^{-7}$ M for antigen and antibody interactions. It was close to the value given by Huang *et al.*,[31] who used an Ag nanoparticle biosensor and quantitatively evaluated the binding kinetics using localized surface plasmon resonance spectra (LSPR). Nevertheless, information on the binding kinetics in cytokine and cytokine inhibitor for anti-cytokine therapy is lacking, especially for that in homogeneous solutions.

Using fluorescence spectroscopy, we successfully investigated the TNFα *vs.* the anti-TNFα binding assay and real time binding kinetics. We described how to purify the dye-labeled conjugates and characterize the binding kinetics quantitatively in homogeneous solution using dual color one-photon fluorescence cross correlation spectroscopy.

2. Experimental

2.1 Materials

The labeling dyes, Alexa Fluor 488-TFP ester and Atto647N NHS ester, were purchased from Invitrogen. Rat TNFα and purified anti-rat TNFα used in the studies were purchased from Cytolab (Peprotech Inc) and Biolegend. In the labeling reaction, reactive dye was dissolved in anhydrous DMSO to enhance the labeling efficiency. Stock TNFα solutions were stored at −20 °C and reconstituted in sterile water to the concentration of 1 mg mL^{-1}.

Conjugation of TNFα and anti-TNFα. In this work, we labeled the recombinant TNFα with amine reactive Alexa Fluor 488-TFP ester (MW 885 Da) and Atto647N NHS ester (MW 843 Da). Alexa Fluor 488 reactive dyes have a TFP ester moiety that is more stable in solution than the commonly used succinimidyl NHS ester. TFP ester reacts efficiently with the primary amine group of TNFα proteins to form a stable dye–protein conjugate. The Atto647N NHS ester also reacts with anti-TNFα to form a conjugate. After conjugates formed, both reactions were blocked by changing the buffer to normal PBS, pH 7.4, by dialysis in a refrigerator at 4 °C.

Purification of dye-labeling conjugates. To avoid hydrolysis during the labeling reaction, the excess free dyes from the labeled proteins were removed using dialysis (3k membrane, according to the instructions of the manufacturer) in phosphate buffer saline (PBS, pH 7.4) at room temperature. The mixtures were then dialyzed overnight at 4 °C against PBS. To separate the free dyes and unlabeled proteins, the mixtures were then purified from reactants using a size exclusion analytical column (BioSep-SEC 2000, Phenomenex) with a guard cartridge. After purification, the conjugates were concentrated using a 10k ultrafiltration membrane (Millipore, USA). For long storage, the conjugates were divided into small aliquots and frozen at −20 °C to avoid repeated freezing and thawing.

Immunoblot analysis. The binding of TNFα to antibodies was performed using the immunoblot technique, Dot Blot method. Here, the reconstituted TNFα and Alexa488 labeled TNFα were spotted directly to the nitrocellulose membrane in various concentrations. Following the blocking with BSA in PBS/Tween-20 (PBST), either pure antibody or Atto647N labeled antibody was incubated separately for 1 h at room temperature. After extensive washing with PBST, the membranes were incubated

with sheep polyclonal anti-mouse antibody (abcam)-HRP conjugated, for 1 h at 1 : 5000 dilutions. After extensive washing, the filters were developed with an enhanced chemiluminescence (ECL) kit for 1 min, following the procedure described by the manufacturer.

Spectroscopy. Steady-state spectra were acquired with a DU800 UV spectrometer (Beckman) and Cary Eclipse Fluorescence spectrometer (Varian). Time resolved fluorescence decay curves of the conjugates were collected using a time correlated single photon counting system (IBH Company, UK). For fluorescence lifetime measurements, the samples placed in the sample chamber were excited at 470 nm with a 1 MHz, ~200 ps wide pulse. Emission photons were first selected by a monochromator (Seya-Namioka type, 200–800 nm) before being detected by the photomultiplier tube module (TBX-04 from IBH, Glasgow, UK) containing the preamplifier and the constant fraction discriminator.

2.2 Experimental setup for single-photon FCS and FCCS

Fig. 1 shows the experimental apparatus. The single-photon FCS and dual-color FCCS experiments were performed with an inverted microscope (Olympus IX71, Tokyo, Japan). The excitation light sources with pulse durations of 50 picoseconds and a repetition rate of 20 MHz for 470 and 635 nm diode lasers (Picoquant GmbH, Berlin, Germany) were combined by a dual line beamsplitter (F53-470, AHF analysentechnik AG) and then introduced into a polarization-maintaining single mode fiber to shape both excitation beams into Gaussian beams. The output beams were then collimated and reflected by a galvanometer scanner of FV300 (Olympus, Tokyo, Japan) and introduced into the microscope. To avoid cross-talk in the time and spectral domains between the two detection channels, 470 nm laser pulses were electronically delayed by 16 ns with respect to the 635 nm laser pulses. A proper dichroic beamsplitter (FF662-FDi01, Semrock) and bandpass filters (FF01-536/40, Semrock, for green channel and HQ-685/70M, Omega Optical, for red channel) were then used to minimize the emission spectral overlap. The 60× water immersion objective of NA 1.2 (Olympus, Tokyo, Japan) was utilized to focus the excitation beams and to collect fluorescence signals from these dye-labeled molecules. A 100 μm confocal pinhole was used to reject out of focus fluorescence. The overall fluorescence signals were acquired by two single photon avalanche photodiodes (APD) (Micro Photon Devices, Bolzano, Italy). The TTL outputs of these two APDs were then coupled into a time correlated single photon counting (TCSPC) device (PicoHarp300, Picoquant GmbH, Berlin, Germany), and latter FCS and FCCS analyses were performed with Symphotime software 5.0 (Picoquant GmbH, Berlin, Germany). To determine the effective volumes of the dual color one-photon FCCS system, calibration of the effective focal volumes for auto correlation and cross correlation curves was achieved by measuring the FCS curves of the fluorescent dyes of Alexa488 and Alexa633 (Invitrogen) for green and red channels, respectively.

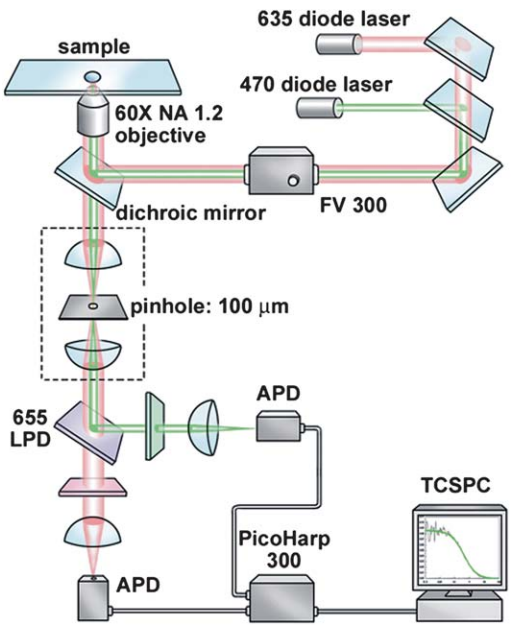

Fig. 1 Schematic diagram of dual-color one-photon fluorescence cross correlation spectroscopy.

Furthermore, in the FCS and FCCS measurements, coverslips of the sample holders were thoroughly cleaned by sonication in methanol and ultrapure water (Millipore) for 30 min, blocked with 2% BSA to reduce non-specific binding, and subsequently stored in PBS solution prior to sample preparation. All measurements were conducted at room temperature.

2.3 Theory of FCS and FCCS

Fluorescence correlation spectroscopy measures the fluctuations of fluorescence intensities of low-concentration diffusing molecules (typically at nanomolar concentrations) within a small focal excitation volume and analyzes the fluctuations using the temporal correlation function to extract molecular mobility and chemical kinetics. At equilibrium, the fluorescence fluctuates about a mean value because of individual molecules diffusing in and out of the focal volume; the fluctuation $\delta F(t)$ of the fluorescence intensity $F(t)$ is defined with the normalized autocorrelation function $G(\tau)$ as

$$G(\tau) = \frac{\langle \delta F(t) \cdot \delta F(t+\tau) \rangle}{\langle F(t) \rangle^2} \quad (1)$$

where $\langle F(t) \rangle$ is the time averaged fluorescence intensity and $\delta F(t + \tau)$ is the fluctuation at a given time $(t + \tau)$ defined as the difference between $F(t)$ and $\langle F(t) \rangle$, τ is a lag time. Similarly, the cross correlation function $G_{ij}(\tau)$ of two fluorescent species, i and j, is described as

$$G_{ij}(\tau) = \frac{\langle \delta F_i(t) \cdot \delta F_j(t+\tau) \rangle}{\langle F_i(t) \rangle \langle F_j(t) \rangle} \quad (2)$$

where $\langle F_i(t) \rangle$ and $\langle F_j(t) \rangle$ are the time averaged fluorescence intensities of species i and j and $\delta F_i(t)$ and $\delta F_j(t + \tau)$ are their fluctuation at time t and $(t + \tau)$. In this study, these two fluorescent species correspond to Alexa 488 labeled TNFα and the Atto647N labeled antibody.

The autocorrelation function decays with time τ, and the shape of the decay and the characteristics of the decay time are related to the mechanisms and rates of the processes that generate the fluctuations of fluorescence. For molecules diffusing freely within

an excitation/detection volume of Gaussian shape, the normalized autocorrelation function is described as[7]

$$G(\tau) = \frac{1}{V_{\text{eff}}\langle C\rangle}\frac{1}{\left(1+\frac{\tau}{\tau_{\text{D}}}\right)}\frac{1}{\sqrt{1+\frac{\tau}{\tau_{\text{D}}k^2}}} \quad (3)$$

where τ_{D} is the average diffusion time of the fluorescent molecules, V_{eff} is the effective detection volume ($V_{\text{eff}} = \pi^{3/2}w_0^2 z_0$, where w_0 and z_0 are the $1/e^2$ of the radial and axial radius of the laser, respectively), $\langle C\rangle$ is the average concentration of molecules in the detection volume, and k is the eccentricity of the confocal volume ($k = z_0/w_0$). Accordingly, the amplitude of the autocorrelation function is inversely related to the average number $\langle N\rangle$ of fluorescent molecules in the detection volume; the parameters $\langle N\rangle$, τ_{D} and k were obtained from the best fit of autocorrelation curves.

In some cases, the fluorescence of molecules is accompanied with radiative transitions of dark states, such as triplet states, due to intramolecular dynamic processes. Because the radiative transitions of the triplet states that occur at a much slower time scale could change the correlation trace, they have to be taken into account. Thus, the autocorrelation function must be modified to

$$G(\tau) = \frac{\left[1-T+Te^{-(t/\tau_{\text{T}})}\right]}{(1-T)}\frac{1}{\langle N\rangle}\frac{1}{\left(1+\frac{\tau}{\tau_{\text{D}}}\right)}\frac{1}{\sqrt{1+\frac{\tau}{\tau_{\text{D}}k^2}}} \quad (4)$$

where T is the fraction of molecules in the triplet state and τ_{T} is the lifetime of the triplet state. Hence, the amplitude of the autocorrelation function at $\tau = 0$, $G(0)$, is related to the average number $\langle N\rangle$ of fluorescent molecules in the detection volume as $G(0) = 1/[\langle N\rangle(1-T)]$.

For the cross correlation function $G_{ij}(\tau)$ that compares the fluorescence signals of the two fluorescent species i and j at different lag times, τ, the equation is given by[22]

$$G_{ij}(\tau) = \frac{\langle C_{ij}\rangle}{V_{\text{eff}}\left(\langle C_i\rangle+\langle C_{ij}\rangle\right)\left(\langle C_j\rangle+\langle C_{ij}\rangle\right)}\frac{1}{\left(1+\frac{\tau}{\tau_{\text{D}}}\right)}\frac{1}{\sqrt{1+\frac{\tau}{\tau_{\text{D}}k^2}}} \quad (5)$$

where $\langle C_i\rangle$, $\langle C_j\rangle$, and $\langle C_{ij}\rangle$ are the concentrations of the fluorescent species i, j and bound molecules ij, respectively. The amplitude of the cross correlation curve at lag time $\tau = 0$, $G_{ij}(0)$, is proportional to the relative concentration of bound species. The absolute concentration can thus be calculated from $G_{ij}(0)$ according to the equation

$$\langle C_{ij}\rangle = \frac{G_{ij}(0)}{V_{\text{eff}}\left(G_i(0)+G_j(0)\right)} \quad (6)$$

where $G_i(0)$ and $G_j(0)$ are the amplitudes of the autocorrelation functions of fluorescent species i and j at time $\tau = 0$, respectively.

In addition to molecular concentrations, the diffusion coefficient D of diffusing molecules can be calculated from the fitted diffusion time τ_{D} according to the equation $\tau_{\text{D}} = w_0^2/4D$ for one-photon excitation. With the given temperature T, the known viscosity η of the medium, and the Boltzmann constant k_{B}, the hydrodynamic radius R_{h} of the diffusing molecules can be evaluated using the Stokes–Einstein equation:

$$D = \frac{k_{\text{B}}T}{6\pi\eta R_{\text{h}}} \quad (7)$$

3. Results and discussion

3.1 Characterizations

In our study, we analyzed the interaction of antigen and its respective antibody. The mobility of the immune complex was also determined with the kinetic parameters. Fig. 2A shows the schematic structures of the immune complex. In the case of the immune reaction by fluorescently labeled TNFα and the antibody, the slow diffusion of the dual color labeled TNFα–anti-TNFα complex can be further observed by monitoring the variation of the FCCS signals.

Purification of the fluorescently labeling conjugates. In the dual color FCCS experiments, the presence of the free dyes and/or unlabeled proteins greatly diminished the amplitude of the cross correlation function. Therefore, accurate purification of the conjugates was necessary. In the conjugation, the TNFα was labeled with amine reactive Alexa Fluor 488-TFP ester and anti-TNFα was labeled with Atto647N NHS ester. Both Alexa488-labeled TNFα and Atto647N-labeled anti-TNFα were purified with size exclusion HPLC. In order to determine precisely the size of the TNFα and the antibody, a series of proteins (the range of MW of 2000 kDa to 16 kDa) were run as size markers (Fig. 3a). Alexa488 labeled TNFα and Atto647N labeled anti-TNFα were purified and analyzed by gel filtration chromatography performed on a size exclusion column (BioSep-SEC-S2000 column), as shown in Fig. 3b. From the chromatogram, native TNFα was eluted from the column in the fraction between conalbumin (75 kDa) and ovalbumin (43 kDa), indicating that the protein is thought to be trimeric in solution. Finally, purified Alexa488-TNFα and Atto647N-anti-TNFα were eluted in the

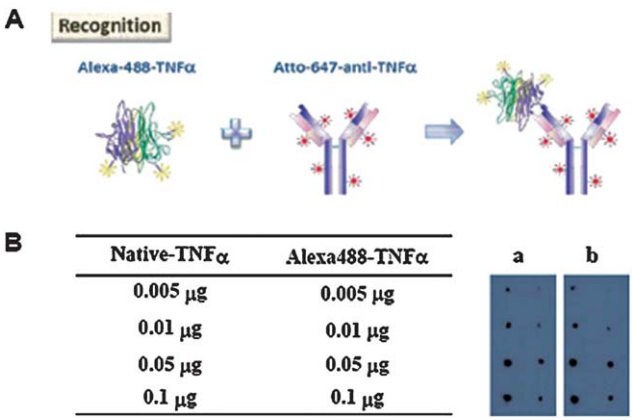

Fig. 2 (A) Binding assay of the fluorescent labeled TNFα and the anti-TNFα. (B) Measurements of binding affinity by Dot Blot analysis by using anti-TNFα to either native TNFα or Alexa488 labeled TNFα at various concentrations; column 'a' represented the TNFα at concentrations at 0.005, 0.01, 0.05 and 0.1 μg and column 'b' represented the Alexa488 labeled TNFα at 0.005, 0.01, 0.05 and 0.1 μg from top to bottom, respectively.

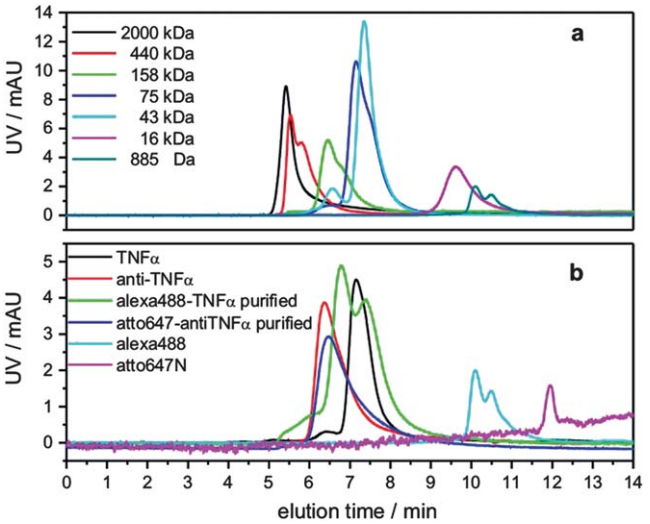

Fig. 3 Size characterization and gel filtration chromatogram of labeled and unlabeled Alexa488-TNFα and Atto647N-anti-TNFα molecules. (a) The size determination of TNFα and anti-TNFα was achieved by gel filtration chromatography on BioSep-SEC-S2000 column. This column was equilibrated with PBS, 1 mL min^{-1}, and calibrated with the following proteins (5 μL of a concentration of 1 mg mL^{-1} protein loaded) were analyzed using 10 mM PBS, pH 7.5, as an elution buffer): blue dextran 2000 (2000 kDa), ferritin (440 kDa), aldolase (158 kDa), conalbumin (75 kDa), ovalbumin (43 kDa), human leptin (16 kDa), and Alexa488 dye (885 Da). (b) Gel filtration chromatogram of the labeled and unlabeled Alexa488-TNFα and Atto647N-anti-TNFα, and free dyes.

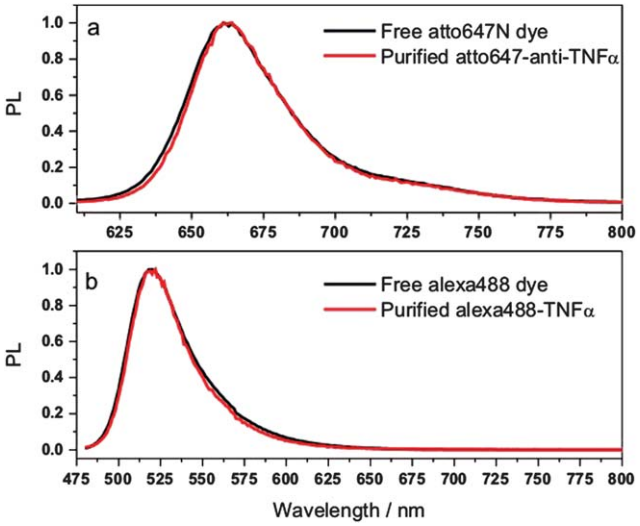

Fig. 4 Fluorescence spectra of free dyes and their conjugates. The top plot is recorded for the fluorescence spectra of Atto647N dye and Atto647N-anti-TNFα-conjugated excited at 600 nm, and the bottom layer is for the Alexa488 and Alexa488-TNFα-conjugated excited at 470 nm, respectively.

6.79 mins and 6.5 mins fractions, respectively, and separated from the free dyes.

Binding affinity. To characterize the binding affinity, the anti-TNFα and Atto647N labeled anti-TNFα were examined for their binding to either TNFα or Alexa488 labeled TNFα by Dot Blot analysis. Fig. 2B shows the results. Non-labeled native TNFα at different concentrations revealed a higher binding affinity to its antibody than fluorescently labeled TNFα. This was determined by comparing the dot signal intensities between Alexa488-labeled TNFα and native TNFα. According to our data, the fluorescent labeling process significantly reduced the binding affinity of the TNFα, which was, presumably, induced from subtle changes in the tertiary structure (conformational change), hydrophobicity or surface charge of the TNFα, at least for the region of the binding site for the antibody.

Fluorescence spectra. Fig. 4 shows the steady state spectra of the conjugates. The figure displays the normalized emission spectra of each conjugate that is similar to the free dye. This suggests that the potential energy surfaces of the conjugates are similar to those of the free dyes after fluorescently labeling. Time resolved fluorescence lifetime measurements were also recorded. The lifetime of the Alexa488 labeled TNFα conjugates is 4.08 ns, which is shorter than the lifetime of the free Alexa488 dye. Even when the combination of the Alexa488-TNFα with Atto647N labeled anti-TNFα occurs, the lifetime of this immune complex is as the same as that of Alexa488-TNFα alone.

3.2 Fluorescence correlation spectroscopy and fluorescence cross correlation spectroscopy

In order to accurately record the diffusion time of the diffusing species, the proper confocal volumes at the focal points for 470 and 635 nm could be obtained by carefully adjusting the collar ring of the objective lens. In our detection system, the detection conditions were optimized by the structure parameter ($k = z_0/w_0$). Using the well-calibrated diffusion coefficient (D) 430 $\mu m^2\ s^{-1}$ for the green channel,[32] and 340 $\mu m^2\ s^{-1}$ for the red channel,[33] we found that the structure parameters of the green and red channels were 6.129 and 5.331 by fitting the FCS data with eqn (4), respectively. Based on these parameters, we calculated the effective volume of the green and red channel to be 0.433 ± 0.009 fL and 0.795 ± 0.015 fL, respectively. The corresponding effective volume for dual color excitation was calculated as 0.607 ± 0.006 fL according to ref. 22.

Single color FCS was then employed to study the diffusion coefficients of Alexa488 labeled TNFα and Atto647N labeled anti-TNFα using 470 nm and 635 nm lasers, respectively. Fig. 5 shows the autocorrelation traces for Alexa488-TNFα and Atto647N-anti-TNFα. The observed diffusion coefficients of the green and red channels were 100.06 ± 4.9 $\mu m^2\ s^{-1}$ and 48.96 ± 2.52 $\mu m^2\ s^{-1}$, respectively. In the analysis, the hydrodynamic diameter $2R_h$ values of the Alexa488-TNFα and Atto647N-anti-TNFα are approximately 4.89 ± 0.24 nm and 9.99 ± 0.52 nm, respectively, which are similar to the mean size of non-labeled TNFα (~5.20 ± 1.23 nm) and non-labeled anti-TNFα (~9.28 ± 0.86 nm). These sizes were determined using light scattering (DLS) equipment (Zetasizer Nano ZS, Malvern Instruments, UK). The findings indicate that the fluorescent labeling process does not significantly influence the hydrodynamic diameter of these proteins.

From previous reports, as pointed out by Jones *et al.*,[34] the three-dimensional crystal structure of human TNFα was

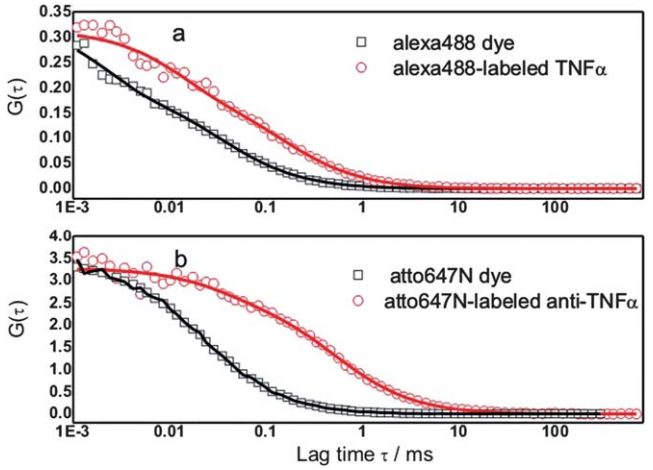

Fig. 5 (a) Autocorrelation curves of Alexa Fluor 488-TFP ester and labeled-TNFα conjugate excited at 470 nm. (b) Autocorrelation curves of Atto647N NHS ester and labeled-anti-TNFα conjugates excited at 635 nm. The line represents the best fit of experimental data; the diffusion coefficients D derived from fitting results are 100.06 ± 4.9 and 48.96 ± 2.52 μm^2 s^{-1} for Alexa488-TNFα and Atto647N-antiTNFα antibody, respectively.

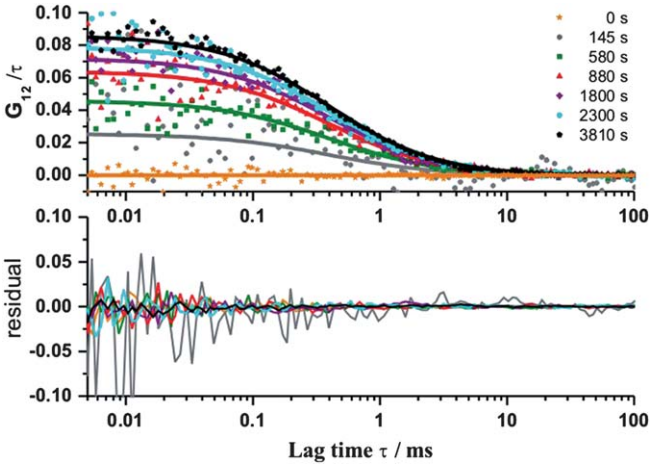

Fig. 6 Time-dependence of cross correlation curves of Alexa488 conjugated TNFα and Atto647N conjugated anti-TNFα and their fitting residuals. Solid lines represent the best fit of experimental data; the concentrations of Alexa488 conjugated TNFα and Atto647N conjugated anti-TNFα are 4.40 nM and 1.88 nM, respectively.

determined to be a compact conical-shaped trimer with an approximate length of 5 nm and maximum breadth 4.5 nm. Our results using chromatography, FCS and DLS measurements all demonstrated that TNFα or Alexa488 labeled TNFα exist in a trimeric form in solution, which is consistent with previous observations from the X-ray crystallographic study of human TNFα. As such, our FCS measurements offer information about the nature of the hydrodynamic diameter of Alexa488-labeled TNFα in a free diffusion state.

3.3 Kinetic analysis of TNFα and anti-TNFα using FCCS

Even though there are two antigen binding sites per antibody, the relatively large molecule size of TNFα (trimeric conformation) at *ca.* 5 nm renders steric hindrance to allow only one TNFα bound to its antibody each time. Therefore, a 1-to-1 binding ratio of TNFα and its antibody is assumed for further calculation of binding kinetics.

Hereof, the formula for data analysis in the recognition reaction

$$\mathrm{A} + \mathrm{B} \underset{k_{\mathrm{off}}}{\overset{k_{\mathrm{on}}}{\rightleftharpoons}} \mathrm{C} \qquad \frac{\mathrm{d}[\mathrm{C}]}{\mathrm{d}t} = k_{\mathrm{on}}[\mathrm{A}][\mathrm{B}] - k_{\mathrm{off}}[\mathrm{C}]$$

is

$$[C(t)] = \frac{k_{\mathrm{on}}[\mathrm{A}]_0[\mathrm{B}]_0}{k_{\mathrm{on}}[\mathrm{A}]_0 + k_{\mathrm{on}}[\mathrm{B}]_0 + k_{\mathrm{off}}}\left(1 - e^{-(k_{\mathrm{on}}[\mathrm{A}]_0 + k_{\mathrm{on}}[\mathrm{B}]_0 + k_{\mathrm{off}})t}\right) \quad (8)$$

where $[A]_0$, $[B]_0$, and [C] indicate the initial concentrations of Alexa488-TNFα and Atto647N-anti-TNFα, and the concentration of the binding pair. In a previous study, we qualitatively confirmed that the dye-labeled proteins interacted with the antibody with a weaker affinity as determined by Dot Blot analysis. To further quantify the change in affinity, we employed dual color FCCS to investigate the interaction between TNFα and anti-TNFα. Here, subnanomolar concentrations of each species were mixed to allow binding and the data were collected for 120 s for each measurement. As shown in Fig. 6, the cross correlation trace of TNFα and the antibody were recorded against lag times within ~40 mins to reach equilibrium in the reaction. The increase in the cross correlation amplitude indicates the growth of the antigen–antibody complex with time. Furthermore, the concentrations of the bound complex in the effective volume were also analyzed with respect to time from the amplitudes of the cross correlation and autocorrelation curves according to eqn (6). Fig. 7 shows the kinetic fitting curve of the bound complexes of Alexa488-TNFα and Atto647-anti-TNFα with the initial concentrations of 3.66 and 1.90 nM, respectively.

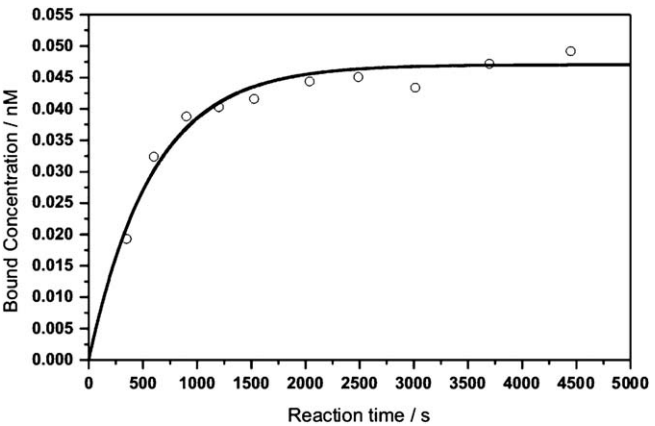

Fig. 7 Concentrations of Alexa488 TNFα/Atto647 anti-TNFα complexes at different reaction times calculated from the amplitudes of cross correlation and autocorrelation curves according to eqn (8). The initial concentrations of Alexa488 TNFα and Atto647 anti-TNFα are 3.66 and 1.90 nM; the solid line represents the best fit of experimental data. Average association (k_{on}) and dissociation (k_{off}) reaction rate constants are (1.13 ± 0.08) × 10^4 M^{-1} s^{-1} and (1.53 ± 0.19) × 10^{-3} s^{-1}, respectively; the corresponding equilibrium dissociation constant (K_{d}) is (1.36 ± 0.10) × 10^{-7} M.

Table 1 Comparison of the reaction rates (k_{on} and k_{off}) and equilibrium dissociation constants (K_d) for the TNFα and anti-TNFα

Source	k_{on}/M^{-1} s^{-1}	k_{off}/s^{-1}	K_d/M
FCCS/This study	$(1.13 \pm 0.10) \times 10^4$	$(1.53 \pm 0.19) \times 10^{-3}$	$(1.36 \pm 0.10) \times 10^{-7}$
SPR/Z8 antibody[a]	470 ± 9.98	$(1.08 \pm 0.08) \times 10^{-4}$	$(2.31 \pm 0.12) \times 10^{-7}$
SPR/Z12 antibody[a]	462 ± 12.5	$(2.49 \pm 0.22) \times 10^{-4}$	$(5.42 \pm 0.49) \times 10^{-7}$
Fiber optics SPR[b]	—	—	1.22×10^{-9}
LSPR[c]	128	1.18×10^{-4}	5.88×10^{-7}

[a] Ref. 30: *Sens. Actuators B*, 2004, **99**, 416. [b] Ref. 29: *Anal. Chem.*, 2005, **77**, 7016. [c] Ref. 31: *J. Am. Chem. Soc.*, 2008, **130**, 17095.

Here, the experimental data were then calculated using eqn (8) to obtain the association (k_{on}), dissociation (k_{off}) rate constants, and equilibrium dissociation constant (K_d). The results were $(1.13 \pm 0.10) \times 10^4$ M^{-1} s^{-1}, $(1.53 \pm 0.19) \times 10^{-3}$ s^{-1}, and $(1.36 \pm 0.10) \times 10^{-7}$ M, respectively. The variability observed is small and demonstrates that the platform is reliable. However, the results from previous published reports from several laboratories given in the Table 1 showed that the equilibrium dissociation constant (K_d) was $(2.31 \sim 5.42) \times 10^{-7}$ M[30] and 5.88×10^{-7} M,[31] the k_{on} was $(1.3 \sim 4.7) \times 10^2$ $M^{-1}s^{-1}$,[30,31] and k_{off} was $(1.08 \sim 2.94) \times 10^{-4}$ s^{-1}.[30,31] Obviously, our kinetic analysis shows slightly larger k_{on}, k_{off}, and K_d values than those reported in heterogeneous environments, which are displaying relatively slower association and dissociation rates. This discrepancy can most likely be explained by two factors; one is that the smaller association constants, k_{on}, obtained from SPR and LSPR methods, were due to depletion of the reactants close to the surfaces, and another is that the slower dissociation constants, k_{off}, by SPR-related methods, was limited by mass transport.[35] However, Battaglia *et al.* reported different K_d values of 1.22×10^{-9} M, based on SPR, which was approximately 100-fold lower than our results. The lack of consistency in the quantitative relationship between SPR-relative reports suggests that the observed kinetic parameter variability is likely attributable to being heterogeneously dependent in liquid–solid interfaces or the concentration of the surface-immobilized antigen.[36]

We further considered if the fluorescence resonance energy transfer (FRET) between the two labeled dyes or the brightness changes of the dyes upon protein binding might affect the accuracy of our FCCS analysis. Although the emission spectrum of Alexa488 partially overlaps the absorption spectrum of Atto647N, FRET efficiency is also greatly determined by other two factors: one is the distance, and the other is the dipole moment between donor and acceptor for the non-radiative energy transfer to occur. In consideration of the molecular size of TNFα (*ca.* 5 nm) and its antibody (*ca.* 10 nm), their combined steric effect likely results in the distance between the two labeled fluorescence dyes in the binding complexes of TNFα-488-antibody-647N larger than 10 nm. Such a spatial separation between donor (Alexa488) and acceptor (Atto647N) greatly decreases their FRET efficiency. It is further evident by the lack of cross correlation that was observed between the autocorrelation functions of green and red channels of the binding complexes while using 470 nm laser for excitation (data not shown). Given that, the FRET efficiency in the dual-labeled binding complexes should be extremely low. Furthermore, according to the K_d values measured in the FCCS experiment, only less than 2% binding complexes formed in the mixture of unbound TNFα and unbound antibody. Thus the brightness changes upon protein binding could not be observed. It is worth noting that our measurement is the first report on the binding kinetics for the anti-TNFα in the homogeneous phase. Our investigation found the recognition of TNFα and anti-TNFα in a free diffusion state mimicking the real immune reaction.

Conclusions

In summary, we have demonstrated for the first time a quantitative approach to real time investigation of the biospecific recognition of fluorescently labeling TNFα and anti-TNFα antibody. We determined the kinetic rate constants and K_d values in a homogeneous system mimicking the real immune reaction using dual color fluorescence cross correlation spectroscopy. Combining the FCCS and implantable microdialytic porous devices, the present work with FCCS can be further extended to measure the *in situ* dynamics of TNFα induction in cerebrospinal fluid following spinal cord injury (SCI). It is clinically important to comprehend the temporal profile of proinflammatory factor induction following SCI; the investigation using FCCS for this purpose is currently undergoing.

Acknowledgements

This study was supported by the Grants MED-099-PP-04 and NM-099-PP-01 from the National Health Research Institutes of Taiwan and grants NSC 95-2120-M-260-002 and Biomedical NanoImaging Core Facility of the National Nanoscience and Nanotechnology Program from the National Science Council of Taiwan.

References

1 B. B. Aggarwal, Signalling pathways of the TNF superfamily: A double-edged sword, *Nat. Rev. Immunol.*, 2003, **3**, 745–756.
2 X. Wang and Y. Lin, Tumor necrosis factor and cancer, buddies or foes?, *Acta Pharmacol. Sin.*, 2008, **29**, 1275–1288.
3 A. Corti, G. Fassina, F. Marcucci, E. Barbanti and G. Cassani, Oligomeric tumour necrosis factor alpha slowly converts into inactive forms at bioactive levels, *Biochem. J.*, 1992, **284**, 905–910.
4 W. M. Kooloos, D. J. de Jong, T. W. Huizinga and H. J. Guchelaar, Potential role of pharmacogenetics in anti-tnf treatment of rheumatoid arthritis and crohn's disease, *Drug Discovery Today*, 2007, **12**, 125–131.
5 G. Ferraccioli and E. Gremese, Thrombogenicity of TNF alpha in rheumatoid arthritis defined through biological probes: TNF alpha blockers, *Autoimmun. Rev.*, 2004, **3**, 261–266.
6 M. Feldmann and R. N. Maini, Lasker clinical medical research award. TNF defined as a therapeutic target for rheumatoid arthritis and other autoimmune diseases, *Nat. Med.*, 2003, **9**, 1245–1250.

7 E. L. Elson, Fluorescence correlation spectroscopy. I. Conceptual basis and theory, *Biopolymers*, 1974, **13**, 1–27.
8 D. Magde, E. L. Elson and W. W. Webb, Fluorescence correlation spectroscopy. II. An experimental realization, *Biopolymers*, 1974, **13**, 29–61.
9 Z. Petrasek and P. Schwille, Precise measurement of diffusion coefficients using scanning fluorescence correlation spectroscopy, *Biophys. J.*, 2008, **94**, 1437–1448.
10 C. B. Muller, A. Loman, V. Pacheco, F. Koberling, D. Willbold, W. Richtering and J. Enderlein, Precise measurement of diffusion by multi-color dual-focus fluorescence correlation spectroscopy, *Europhys. Lett.*, 2008, **83**, 46001.
11 J. Enderlein, I. Gregor, D. Patra, T. Dertinger and U. B. Kaupp, Performance of fluorescence correlation spectroscopy for measuring diffusion and concentration, *ChemPhysChem*, 2005, **6**, 2324–2336.
12 C. Gell, D. J. Brockwell, G. S. Beddard, S. E. Radford, A. P. Kalverda and D. A. Smith, Accurate use of single molecule fluorescence correlation spectroscopy to determine molecular diffusion times, *Single Mol.*, 2001, **2**, 177–181.
13 J. Korlach, P. Schwille, W. W. Webb and G. W. Feigenson, Characterization of lipid bilayer phases by confocal microscopy and fluorescence correlation spectroscopy, *Proc. Natl. Acad. Sci. U. S. A.*, 1999, **96**, 8461–8466.
14 U. Haupts, S. Maiti, P. Schwille and W. W. Webb, Dynamics of fluorescence fluctuations in green fluorescent protein observed by fluorescence correlation spectroscopy, *Proc. Natl. Acad. Sci. U. S. A.*, 1998, **95**, 13573–13578.
15 K. Chattopadhyay, S. Saffarian, E. L. Elson and C. Frieden, Measurement of microsecond dynamic motion in the intestinal fatty acid binding protein by using fluorescence correlation spectroscopy, *Proc. Natl. Acad. Sci. U. S. A.*, 2002, **99**, 14171–14176.
16 H. D. Kim, G. U. Nienhaus, T. Ha, J. W. Orr, J. R. Williamson and S. Chu, Mg^{2+}-dependent conformational change of RNA studied by fluorescence correlation and FRET on immobilized single molecules, *Proc. Natl. Acad. Sci. U. S. A.*, 2002, **99**, 4284–4289.
17 R. Rigler, A. Pramanik, P. Jonasson, G. Kratz, O. T. Jansson, P. Nygren, S. Stahl, K. Ekberg, B. Johansson, S. Uhlen, M. Uhlen, H. Jornvall and J. Wahren, Specific binding of proinsulin c-peptide to human cell membranes, *Proc. Natl. Acad. Sci. U. S. A.*, 1999, **96**, 13318–13323.
18 R. Brock, G. Vamosi, G. Vereb and T. M. Jovin, Rapid characterization of green fluorescent protein fusion proteins on the molecular and cellular level by fluorescence correlation microscopy, *Proc. Natl. Acad. Sci. U. S. A.*, 1999, **96**, 10123–10128.
19 J. C. Politz, E. S. Browne, D. E. Wolf and T. Pederson, Intranuclear diffusion and hybridization state of oligonucleotides measured by fluorescence correlation spectroscopy in living cells, *Proc. Natl. Acad. Sci. U. S. A.*, 1998, **95**, 6043–6048.
20 U. Meseth, T. Wohland, R. Rigler and H. Vogel, Resolution of fluorescence correlation measurements, *Biophys. J.*, 1999, **76**, 1619–1631.
21 M. Eigen and R. Rigler, Sorting single molecules: Application to diagnostics and evolutionary biotechnology, *Proc. Natl. Acad. Sci. U. S. A.*, 1994, **91**, 5740–5747.
22 P. Schwille, F. J. Meyer-Almes and R. Rigler, Dual-color fluorescence cross-correlation spectroscopy for multicomponent diffusional analysis in solution, *Biophys. J.*, 1997, **72**, 1878–1886.
23 D. M. Jameson, J. A. Ross and J. A. Albanesi, Fluorescence fluctuation spectroscopy: Ushering in a new age of enlightenment for cellular dynamics, *Biophys. Rev.*, 2009, **1**, 105–118.
24 L. C. Hwang and T. Wohland, Recent advances in fluorescence cross-correlation spectroscopy, *Cell Biochem. Biophys.*, 2007, **49**, 1–13.
25 K. Bacia, S. A. Kim and P. Schwille, Fluorescence cross-correlation spectroscopy in living cells, *Nat. Methods*, 2006, **3**, 83–89.
26 P. C. Weber, D. H. Ohlendorf, J. J. Wendoloski and F. R. Salemme, Structural origins of high-affinity biotin binding to streptavidin, *Science*, 1989, **243**, 85–88.
27 L. T. Varghese, R. K. Sinha and J. Irudayaraj, Study of binding and denaturation dynamics of igg and anti-igg using dual color fluorescence correlation spectroscopy, *Anal. Chim. Acta*, 2008, **625**, 103–109.
28 F. Fujii, M. Horiuchi, M. Ueno, H. Sakata, I. Naga, M. Tamura and M. Kinjo, Detection of prion protein immune complex for bovine spongiform encephalopathy diagnosis using fluorescence correlation spectroscopy and fluorescence cross-correlation spectroscopy, *Anal. Biochem.*, 2007, **370**, 131–141.
29 T. M. Battaglia, J. F. Masson, M. R. Sierks, S. P. Beaudoin, J. Rogers, K. N. Foster, G. A. Holloway and K. S. Booksh, Quantification of cytokines involved in wound healing using surface plasmon resonance, *Anal. Chem.*, 2005, **77**, 7016–7023.
30 Y. Liu, W. Zhang, X. Yu, H. Zhang, R. Zhao, D. Shangguan, Y. Li, B. Shen and G. Liu, Quartz crystal biosensor for real-time monitoring of molecular recognition between protein and small molecular medicinal agents, *Sens. Actuators, B*, 2004, **99**, 416–424.
31 T. Huang, P. D. Nallathamby and X. H. Xu, Photostable single-molecule nanoparticle optical biosensors for real-time sensing of single cytokine molecules and their binding reactions, *J. Am. Chem. Soc.*, 2008, **130**, 17095–17105.
32 J. M. Nitsche, H. C. Chang, P. A. Weber and B. J. Nicholson, A transient diffusion model yields unitary gap junctional permeabilities from images of cell-to-cell fluorescent dye transfer between Xenopus oocytes, *Biophys. J.*, 2004, **86**, 2058–2077.
33 P. Kapusta, *Absolute diffusion coefficients: Compilation of reference data for FCS calibration*, Application note, 2010.
34 E. Y. Jones, D. I. Stuart and N. P. Walker, Structure of tumour necrosis factor, *Nature*, 1989, **338**, 225–228.
35 M. Stenberg and H. Nygren, Kinetics of antigen–antibody reactions at solid–liquid interfaces, *J. Immunol. Methods*, 1988, **113**, 3–15.
36 H. Nygren and M. Stenberg, Immunochemistry at interfaces, *Immunology*, 1989, **66**, 321–327.

